ZnO etching and microtunnel fabrication for high-reliability MEMS acoustic sensor

Mahanth Prasad[1], V. Sahula[2], *Senior Member, IEEE,* and V.K. Khanna[1]

***Abstract*—This paper describes a technique for uniform step coverage of Al on ZnO film in the fabrication of MEMS acoustic sensor. The MEMS acoustic sensors were fabricated by etching ZnO layer in three different etchants: HCl, NH_4Cl with electrolytically-added copper ions and NH_4OH with electrolytically-added copper ions. For the first time, a technique is reported which uses aqueous NH_4OH solution with electrolytically-added copper ions for etching of ZnO layer. For reliable operation of the device, the electrical testing of Al step coverage on ZnO layer was performed. The maximum currents drawn across Al-deposited ZnO edge etched by HCl, Cu added NH_4Cl, and Cu added NH_4OH were 40 mA, 2.5 A and 3.0 A respectively, without any damage to the structures. The investigation shows that uniform Al step coverage on ZnO layer was obtained in case of NH_4OH with electrolytically-added copper ions. During fabrication of the device, a novel technique for building a microtunnel for pressure compensation was also developed. This microtunnel is used to compensate the pressure applied on the silicon diaphragm by connecting the cavity to the atmosphere. To realize the smooth inlet of microtunnel in the cavity, photoresist SU8 was used for patterning the cavity after microtunnel etching. The developed technique for microtunnel fabrication reduces the process complexity and thus improves yield of the device. The packaged device performed satisfactorily in the sound pressure level (SPL), 120-160 dB, over a wide frequency range 30-8000 Hz. The maximum sensitivity of the sensor was measured as 380 µV/Pa.**

***Index Terms*—Electrolytic copper addition, ZnO film, bulk micromachining, Si-diaphragm, TMAH.**

I. INTRODUCTION

Piezoelectric zinc oxide (ZnO) films have played an important role in the field of microelectromechanical systems (MEMS), both bulk micromachined [1], [2] and surface micromachined [3], [4], due to their piezoelectric properties and excellent compatibility with various substrate materials [5]. ZnO films have been used in MEMS devices such as film-bulk acoustic-wave resonators [6], surface-acoustic-wave resonators [7], and acoustic sensors [8], [9]. Many deposition techniques have been developed for deposition of high-quality ZnO films, such as plasma-enhanced chemical-vapor deposition (PECVD) [10], [11], vacuum sputtering [12], [13], molecular beam epitaxy [14], pulsed laser deposition [15], [16] and metal-organic chemical-vapor deposition [17]. While fabricating ZnO-based devices, where the film thickness is higher (>1.0 µm) [18], [19], the fine patterning of the film with positive slope is difficult. In order to etch ZnO layer with fine pattern, a number of dry etching techniques have been reported [20]-[23]. However, a metal mask is required in these techniques to etch ZnO layer, because photoresist gets decomposed when exposed to plasma for long durations [20]. After ZnO etching from an unwanted area, it is difficult to remove the metal mask because most metal etchants attack ZnO. Instead, a wet etching technique with a photoresist mask is always preferred to pattern ZnO films. Moreover, compared with dry etching, the wet etching technique has the advantages of simplicity and low cost. The wet etching of polycrystalline ZnO film deposited by sputtering technique, with different acids and bases, such as HCl, H_2SO_4, HBr, HNO_3, and H_3PO_4 [24], [25], produces negative slope or hanging structures at the edge of the ZnO layer because the lateral etch rate is several times higher than the vertical etch rate due to preferential orientation of the grain. This leads to a major problem of step coverage during fabrication of devices [26], [27]. In [26] and [27], the ZnO etching was done using NH_4Cl with electrolytically-added copper ions but the effects of copper addition was not reported. Also in [27], the electrical testing of Al step coverage on ZnO was not given.

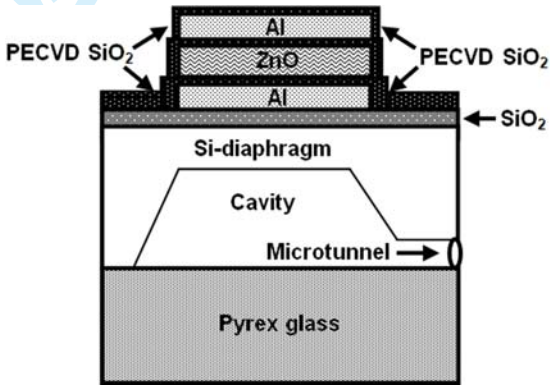

Figure 1: Schematic view of MEMS acoustic sensor.

In this paper, the ZnO-based MEMS acoustic sensor was fabricated by etching ZnO layer in three different solutions: HCl, NH_4Cl with electrolytically-added copper ions and a novel etchant, NH_4OH with electrolytically-added copper ions, separately. The etching properties of ZnO films and electrical testing of fabricated structures by these solutions were studied. Herein, NH_4OH solution with electrolytically-added copper ions is proposed as a promising etchant for ZnO etching because of its uniform and controllable ZnO etching. Most

[1]CSIR-Central Electronics Engineering Research Institute, Pilani – 333031 (Rajasthan), India, Email: vkk_ceeri@yahoo.com.

[2]Malaviya National Institute of Technology, Jaipur, India, Email: sahula@ieee.org

Corresponding author: Mahanth Prasad, Phone: +91-1596-252332, Fax: +91-1596-242294, E-mail: mahanth.prasad@gmail.com

strong acids dissolve ZnO, even at low concentration, due to hydronium (H_3O^+) ions attacking the oxygen in ZnO [28]. In comparison to strong acids, a weak acid NH_4Cl can provide a proper level of hydronium ion concentration for controlled etching of ZnO layer. In a similar way, a weak base NH_4OH with copper ions in the solution can etch ZnO layer in a controlled manner. The present research on ZnO films mainly focuses on how to etch ZnO film with excellent etch front slope and etch rate. However, the ZnO films are reactive materials and sensitive to temperature, acids, bases and even water [5]. By suspending the ZnO deposited samples in the horizontal direction in a 20%NH_4Cl solution, positive slope ($\sim 90°$) was obtained at the edge of the ZnO film [26]. Therefore, for better etch front slope, the samples were kept in the horizontal direction in different etching solutions. A schematic view of ZnO-based MEMS acoustic sensor is shown in Figure 1. The structure consists of a ZnO film covered with thin PECVD SiO_2 layer from both top and bottom sides. The SiO_2-ZnO-SiO_2 structure itself is sandwiched between aluminium electrodes. The complete structure Al-SiO_2-ZnO-SiO_2-Al lies over 25 μm-thick silicon diaphragm covered with 0.5 μm-thick thermal SiO_2 layer. A microtunnel which relates the cavity to the atmosphere is used for pressure compensation. The microtunnel fabrication involves a complex process, which needs simplification.

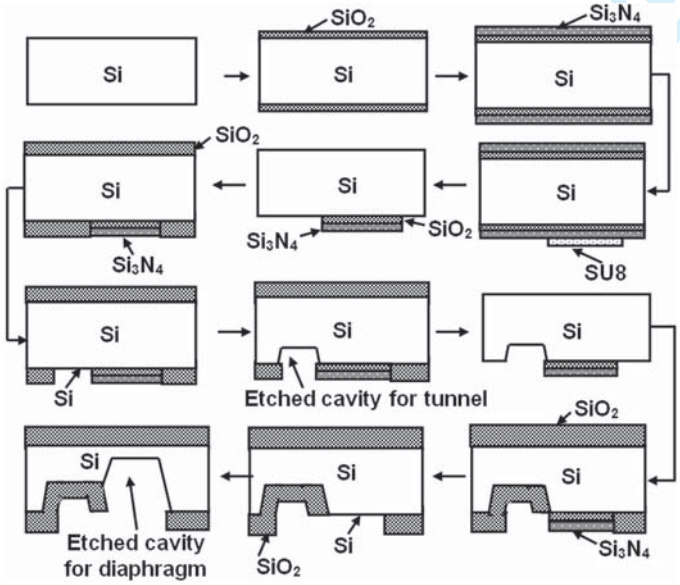

Figure 2: Process flow up to tunnel opening in the Si-cavity.

In recent years, microtunnels have been widely used in microfluidic and microelectromechanical systems [32-33]. Bhusary et al. [34] has demonstrated the fabrication of air channel structures for microfluidic, microelectromechanical and microelectronic applications. In MEMS acoustic sensor, microtunnel is used to compensate the applied pressure on diaphragm. Different materials have been used by researchers to fabricate the microchannels: like polynorbornene (PNB) [34], zeolite [35], silicon [36] and SU8 [37]. The fabrication of microtunnel in these materials besides silicon is mostly incompatible with CMOS processing because these resists cannot withstand the required high temperatures (800-1100ºC). Arora et al. [38] have fabricated a microtunnel for pressure compensation along with a deep cavity in silicon for MEMS acoustic sensor. Reference [38] is the only paper describing tunnel fabrication for pressure compensation in MEMS acoustic sensor using planar silicon wafer. In remaining research papers, acoustic holes are made.

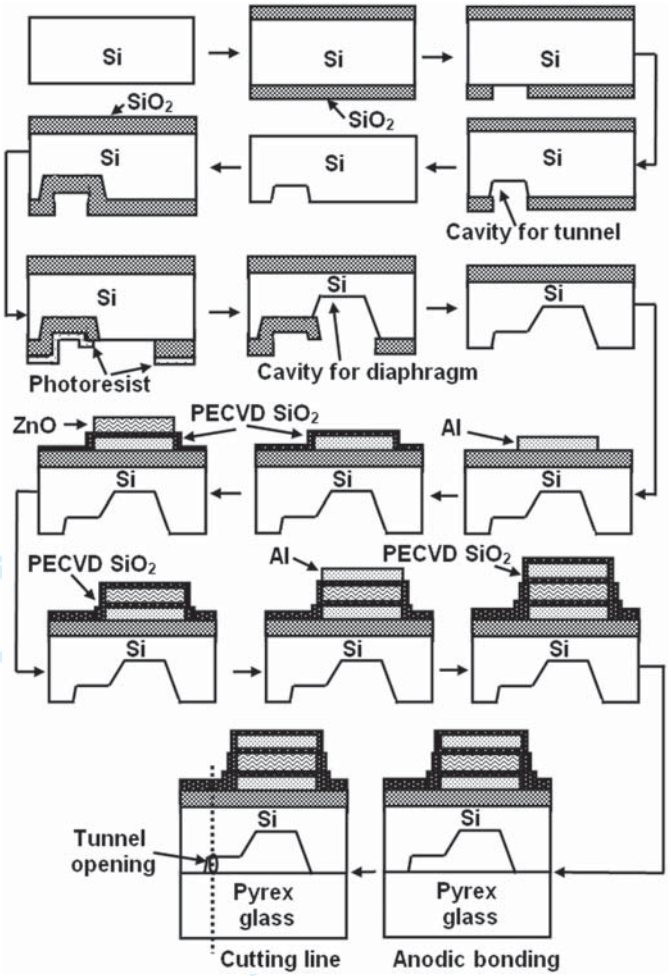

Figure 3: Fabrication flow for ZnO-based MEMS acoustic sensor.

The process flow up to tunnel opening in the cavity introduced in [38] is shown in Figure 2. The following problems exist in aforesaid process: (i) The large number of fabrication steps in this lengthy process, severely degrades the final yield of acoustic sensor chips, (ii) The microtunnel is designed in a way that it slightly overlaps the diaphragm area. During silicon dioxide removal from microtunnel area, the buffered hydrofluoric acid (BHF) also attacks the overlapping area and damages LPCVD silicon nitride covering the diaphragm area. Therefore, in diaphragm fabrication most of the cavities have non-uniform etch depth because overlapping area is already etched up to the depth of microtunnel, creating holes in diaphragms. (iii) During etching of oxide layer (below silicon nitride) from diaphragm area, the silicon dioxide from

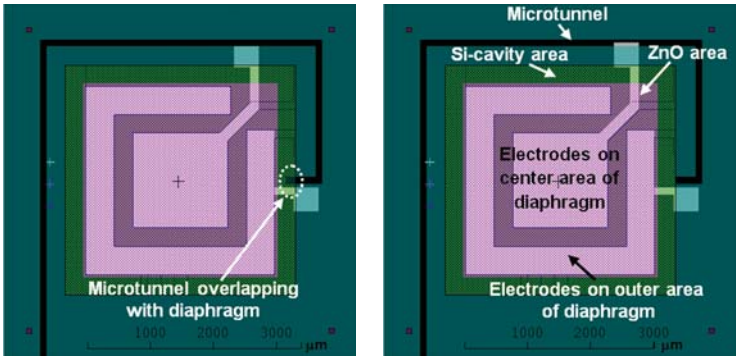

(a) (b)

Figure 4: Mask layout of acoustic sensor using: (a) earlier technique, and (b) proposed technique.

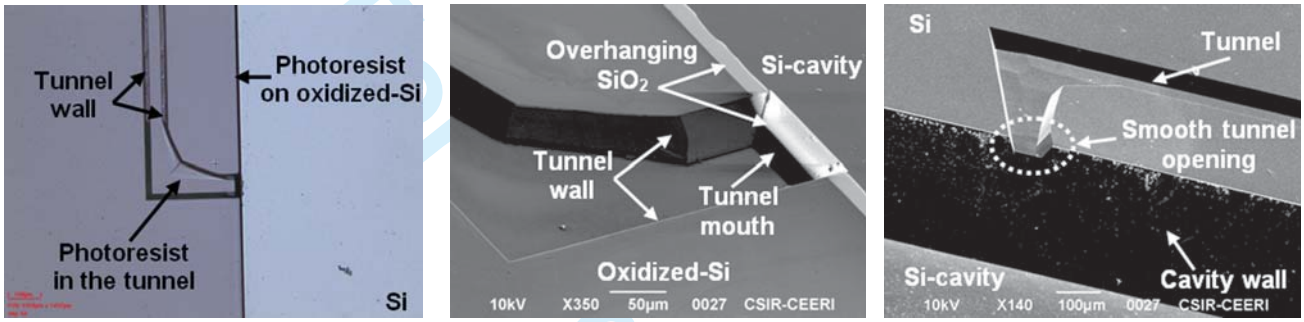

(a) (b) (c)

Figure 5: Bulk micromachining of silicon for diaphragm fabrication: (a) tunnel covered with SU8-2025, (b) lateral etching of silicon in TMAH solution, and (c) structure after removal of overhanging SiO_2 layer.

other areas including tunnel is also removed at the same rate. Therefore, the thickness of the masking layer silicon dioxide is reduced which creates holes in diaphragm as well as in microtunnel during deep cavity etching. (iv) LPCVD silicon nitride is mandatory in this technique which increases process complexity.

This paper presents a novel technique: (1) to avoid the pin holes in silicon diaphragm, (2) to avoid the LPCVD silicon nitride deposition, and (3) reduces the total number of process steps from 21 to 17 in fabrication of MEMS acoustic sensor. The paper is organized as follows. We elaborate a novel technique for microtunnel formation and device fabrication by etching ZnO layer in different etchants in Section-II. The discussion of results are given in Section-III. We conclude in Section-IV.

II. Experimental

The fabrication flow of the MEMS acoustic sensor including proposed technique for microtunnel formation is shown in Figure 3. The microtunnel opening in the cavity is fabricated from step 1 to 8. ZnO patterning and etching are done in step 12. The complete fabrication of the device consists of six masks as follows-mask#1 for microtunnel, mask#2 for Si-diaphragm, mask#3 for bottom electrodes, mask#4 for ZnO patterning, mask#5 for top electrodes and mask#6 for pad opening. For optimum sensitivity of the device, two capacitors of values 80 pF and 140 pF were located on center and outer edge of the diaphragm respectively. Microtunnel width and silicon diaphragm area were taken as 100 µm and 3 mm × 3 mm respectively. The fabrication of acoustic sensor was started with 4-inch *P*-type <100> silicon wafers. The resistivity of wafers was 10-20 ohm.cm. Oxidation of these wafers was done at 1000ºC. The thickness of SiO_2 layer was measured using Dektak 6M surface profiler and found to be 0.5 µm.

In Subsection-A, novel technique for microtunnel fabrication is described. Subsections-B, C and D present the fabrication of device by etching ZnO in different etchants.

A. *Microtunnel fabrication*

The process flow for tunnel opening in the cavity using the proposed technique is shown in Figure 3 (up to step no.8). The mask layout for microtunnel fabrication using earlier [38] and proposed techniques are shown in Figure 4(a) and 4(b) respectively. As can be seen from Figure 4(b), there is no overlap between cavity and channel. The absence of overlapping area between diaphragm and tunnel reduces the number of unnecessary process steps from 12 (Figure 2) to 08 (Figure 4). In earlier technique, the microtunnel was slightly penetrating the diaphragm area whereas in proposed technique, the microtunnel structure ends at the edge boundary of the diaphragm.

The fabrication of microtunnel was started with patterning the oxidized-Si wafers using mask#1. Thermally grown SiO_2 layer from tunnel area was removed by BHF. After removal of SiO_2 layer, bulk micromachining of silicon was done for microtunnel using 25% tetra methyl ammonium hydroxide (TMAH) solution. The etching time and temperature of solution were kept as 2 hours 25 min and 70ºC respectively. A smooth structure, 35.2 µm-deep and 100 µm-wide has been successfully fabricated in silicon substrate. After fabricating the structure for microtunnel, silicon dioxide layer (1.2 µm) was grown at 1000ºC. This layer acts as a masking layer during deep cavity etching. Firstly, photoresist S1818 was tried to protect the microtunnel area during diaphragm patterning. It was observed that the structure is damaged during cavity etching for diaphragm formation, the reason being incomplete step coverage of microtunnel structure using photoresist S1818. Even use of thin photoresist S1813 and thick photoresist SU8-2010 could not improve results.

Finally, photoresist SU8-2025 was tried while patterning the cavity area for silicon diaphragm. It was found that the 35.2 µm-deep and 100 µm-wide acoustic microtunnel structure including curved areas, was completely covered with photoresist SU8-2025, as shown in Figure 5(a). Reactive ion etching (RIE) process was tried for removal of silicon dioxide from the diaphragm area. Consequently, a sharper well-defined boundary of diaphragm area is formed after removal of silicon dioxide. After removal of SiO_2 layer from diaphragm, a cavity of approximately 480 µm depth was etched in 25% TMAH solution for formation of silicon diaphragm. In the present paper, the mask design for microtunnel and diaphragm does not make the alignment critical because lateral etching of silicon in TMAH is sufficient to open the tunnel to the cavity. This can be seen from Figure 5(b), where the silicon has been laterally etched and overhanging SiO_2 is left behind. Etch rate of the 25% TMAH solution at 70ºC was determined for (100) plane to be 15 µm/hr and for (111) as 1.3 µm/hr. The undercut per unit depth was found to be 0.106. The silicon dioxide from back side of wafers was removed for anodic bonding. Figure 5(c) shows the SEM image of backside of structure after removal of overhanging SiO_2 layer. It was observed that the microtunnel is smoothly opened in the cavity. After successful fabrication of tunnel opening in the cavity, the two capacitors, one on the center (∼80 pF) and another on the outer edge (∼140 pF) of the diaphragm were fabricated. For this purpose, Al of 1.0 µm thickness was deposited on front side of these wafers using sputtering technique. Patterning of Al was done using mask#3 for bottom electrode. Then, PECVD SiO_2 of approximately 0.3 µm-thickness was deposited. After PECVD SiO_2 deposition, these wafers were subjected to ZnO deposition.

A highly *c*-axis oriented ZnO film was deposited by RF magnetron sputtering technique with a zinc target (with purity of 99.99%). The process parameters were as follows: sputtering power = 550 W, pressure = 20 mtorr, gas composition = Ar and O_2 in 40 : 60 ratio and deposition time = 5 hours. Thickness of ZnO layer was measured by creating a step in the film and found to be 3.0-3.5 µm. The XRD pattern of ZnO thin film on a bare silicon wafer is shown in Figure 6. The only one peak corresponding to (002) reflection of wurtzite phase of ZnO shows the film growth highly oriented along *c*-axis normal to the substrate. At an angle of 2θ = 34.4º, the ZnO film grains have good orientation. After deposition, photolithography was done on these wafers using mask#4 for ZnO etching. ZnO film has the dimension 3.1 mm × 3.1 mm. The ZnO layer was then etched in different solutions as follows:

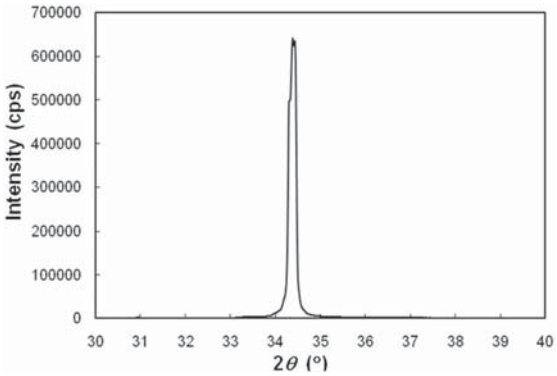

Figure 6: XRD pattern of 3.0 µm-thick ZnO film.

B. Fabrication of device by etching ZnO in HCl

First, HCl was used to etch ZnO film at different solution concentrations (the process was carried out at room temperature). The chemical reaction of ZnO [29], [30] can be described by (1).

$$ZnO + 2HCl = Zn^{2+} + 2Cl^{-} + H_2O \quad (1)$$

It is observed from above equation that the strong acid attacks the oxygen in ZnO and reduces ZnO to Zn. The generation of hydronium ions with solution concentration in case of HCl is shown in Figure 7(a). It is observed that at very low concentration (0.05%) of solution, the hydronium ion concentration is 0.0116228 mole/L. As we increase the solution concentration, the concentration of hydronium ions increases. The hydronium ion concentrations at 2% solution concentration is found to be 0.199526 mole/L. This implies that the number of hydronium ions increases with increasing solution concentration which leads to uncontrolled ZnO etching even at lower concentration of solutions in case of strong acids. The variation of ZnO etch rate in case of HCl is plotted in Figure 7(b). It is found that the etch rate increases with increasing concentration of acid solution. During fabrication of device, the ZnO layer was etched in 0.25% HCl solution concentration. After etching ZnO, 0.3 µm-thick PECVD SiO_2 and then 1.0 µm-thick Al layer for top electrodes were deposited . The passivation layer deposition and then RIE for pad opening were done. Finally, anodic bonding was done before dicing.

C. Fabrication of device by etching ZnO in NH_4Cl solution with Cu addition

Now, the NH_4Cl was used to etch ZnO film at different solution concentrations (the process was carried out at room

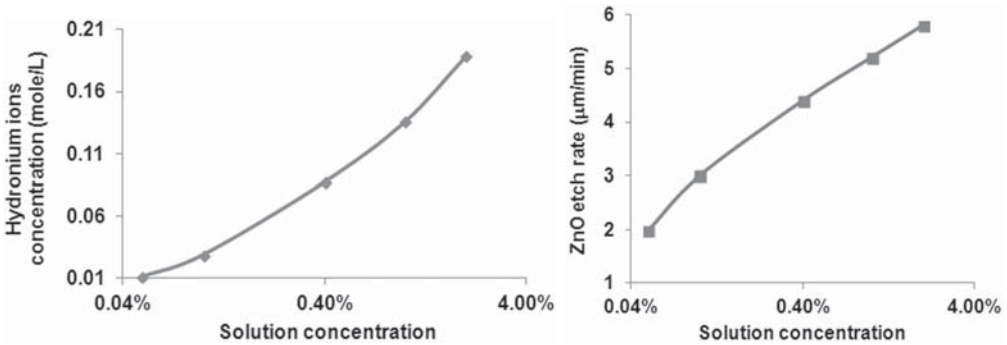

(a) (b)

Figure 7: ZnO etching in HCl solution: (a) variation of hydronium ion concentration with solution concentration, and (b) variation of ZnO etch rate with solution concentration.

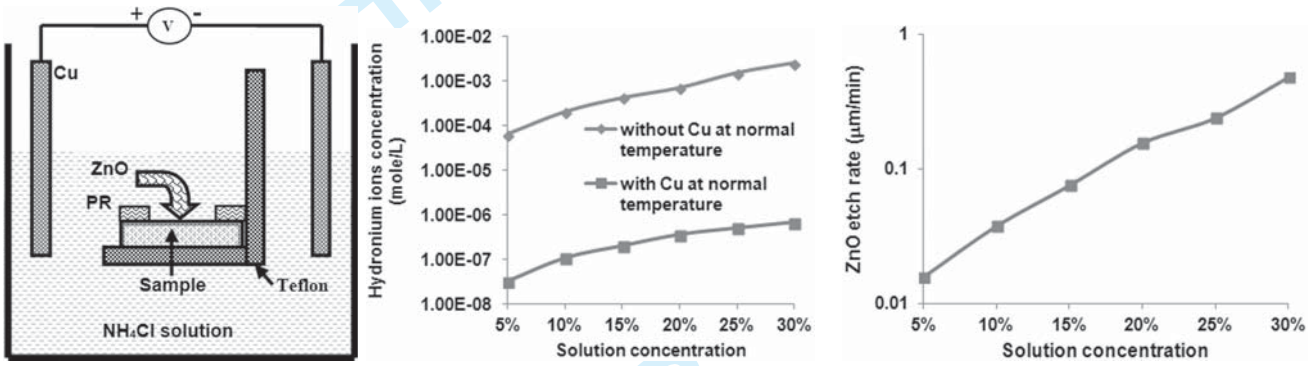

(a) (b) (c)

Figure 8: ZnO etching in NH_4Cl solution: (a) etching setup for electrolytic addition of copper, (b) variation of hydronium ions with solution concentration (with and without Cu-added ions), and (c) variation of ZnO etch rate in NH_4Cl with Cu-added ions at different solution concentrations.

temperature). NH_4Cl solutions of different concentration were prepared by dissolving NH_4Cl powder (99.99% purity) in deionized water. The reactions of ZnO solid state with NH_4Cl solution as described in [31], are reproduced in following set of equations:

$$4NH_4Cl_{(aq)} = 4NH_4^+{}_{(aq)} + 4Cl^-_{(aq)} \quad (2)$$

$$4NH_4^+{}_{(aq)} + 4H_2O = NH_{3(aq)} + 4H_3O^+ \quad (3)$$

$$ZnO_{(s)} + 2H_3O^+ = Zn^{2+}_{(aq)} + 3H_2O \quad (4)$$

Increased concentration of solution results in larger number of hydronium ions. For electrochemical etching of ZnO layer, copper ions were added to NH_4Cl solution in an electrolytic cell [Figure 8(a)]. The electrolytic cell consisted of two parallel electrodes, one for anode and another for cathode. An electrical current was passed through the solution until the solution became blue in color, indicating that copper has been electrolytically-added to the solution. In order to get a good etch front slope of ZnO layer, an etching setup [26], was prepared and the etching experiments were done by suspending the wafers in horizontal direction in the aqueous NH_4Cl solution with electrolytically-added copper ions. The reaction of ZnO (solid state) with electrolytically-added copper ions in NH_4Cl solution, described in [28], is reproduced in the following set of equations:

$$NH_4Cl = NH_4^+{}_{(aq)} + Cl^-_{(aq)} \quad (5)$$

$$NH_4^+{}_{(aq)} + H_2O_{(aq)} = NH_{3(aq)} + H_3O^+. \quad (6)$$

$$Cu \rightarrow Cu^{2+} + 2e^- \quad (7)$$

$$ZnO + 2H_3O^+ = Zn^{2+}_{(aq)} + 3H_2O \quad (8)$$

$$Zn^{2+}_{(aq)} + 4NH_{3(aq)} = [Zn(NH_3)_4]^{2+}_{(aq)}(Clear) \quad (9)$$

$$Cu^{2+}_{(aq)} + 4NH_{3(aq)} = [Cu(NH_3)_4]^{2+}_{(aq)}(Blue) \quad (10)$$

$$[Cu(NH_3)_4]^{2+}_{(aq)} + 2e^- \rightarrow Cu + 4NH_{3(aq)}. \quad (11)$$

Figure 8(b) shows the variation in hydronium ion generation with solution concentration. It is observed that the hydronium ion concentration in copper added solution (=3.5×10^{-7} mole/L) is 1995 times less than in the solution without copper ions (= 6981.1×10^{-7} mole/L) for 20% concentration at normal temperature. Therefore, the experiment without Cu addition discontinued. The ZnO etch rate with solution concentration at normal temperature in case of NH_4Cl solutions with

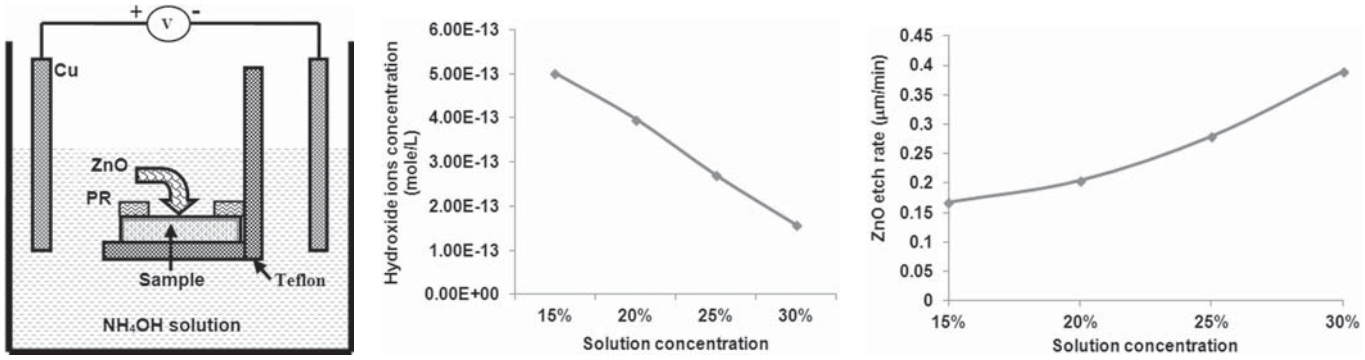

(a) (b) (c)

Figure 9: ZnO etching in NH_4OH solution: (a) etching setup for electrolytic addition of copper in solution, (b) variation of hydroxide ions with Cu-added solution concentration, and (c) variation of ZnO etch rate with Cu-added solution concentration.

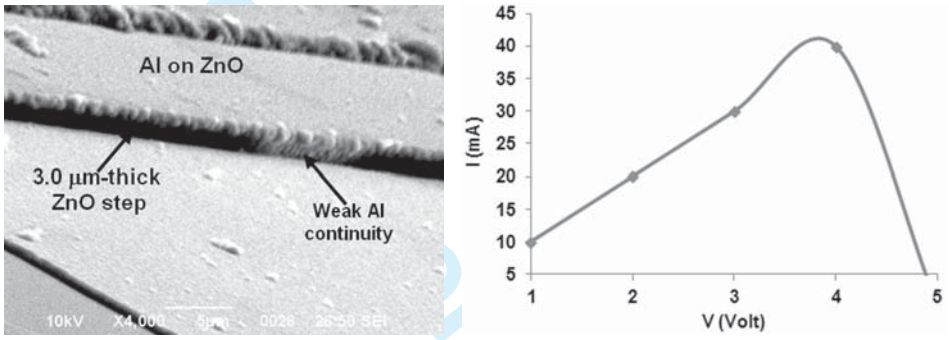

(a) (b)

Figure 10: Electrical testing of structure fabricated by etching ZnO in HCl solution: (a) SEM photograph of the structure, and (b) *I-V* characteristic of Al deposited on ZnO step.

copper addition is plotted in Figure 8(c). It is observed that the etch rate increases with increasing solution concentration. A good etch rate of 0.18 μm/min was obtained at 20% solution concentration. For controlled ZnO etching, a low concentration of hydronium ions is desired [28]. Therefore, we have selected 20% concentration of solution, and the ZnO layer was etched in this solution during fabrication of device. After etching ZnO layer using this solution, the remaining process steps were completed using process flowchart (Figure 3).

D. Fabrication of device by etching ZnO in NH_4OH solution with Cu addition

30% NH_4OH solution was used for ZnO etching but the etching rate was too small, approximately 0.3 μm/hour. Therefore, for ZnO etching, a weak base NH_4OH solution with electrolytically-added copper ions [Figure 9(a)] was proposed. The blue color of solution was observed, implying the generation of compound $[Cu(NH_3)_4]^{2+}{}_{(aq)}$(Blue). Now, ZnO-deposited wafers were etched in this solution by suspending them in horizontal direction. The variation of hydroxide ion concentration of the NH_4OH solution with Cu-added ions was measured at different concentration; the same is shown in Figure 9(b).

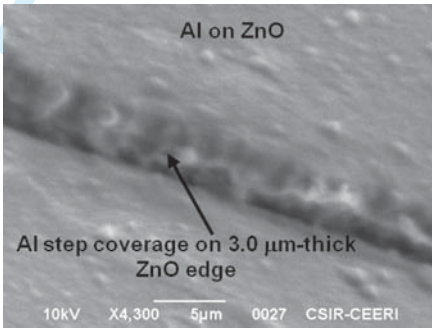

Figure 11: Al step coverage on ZnO edge produced by NH_4Cl with electrolytically-added Cu ions

It was observed that when the concentration increases from 15% to 25%, there is a small variation in hydroxide ion concentration (= 5.0×10^{-13} mole/L to 2.5×10^{-13}mole/L) in comparison to NH_4Cl with electrolytically-added Cu ions (= 2.0×10^{-7} mole/L to 5.0×10^{-7}mole/L). Also, the hydroxide ion concentration in case of NH_4OH with electrolytically-added Cu ions (= 3.98×10^{-13} mole/L) is very small in comparison to hydronium ion concentration in case of Cu added

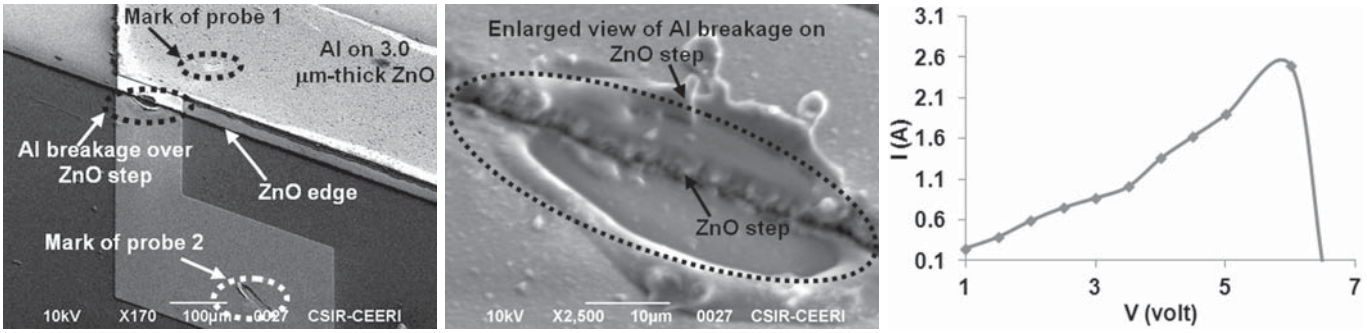

(a) (b) (c)

Figure 12: Electrical testing of structure fabricated by etching ZnO in 20% NH_4Cl solution with electrolytically-added Cu ions: (a) SEM photograph of the structure after passing high current, (b) enlarged view of Al breakage on ZnO step, and (c) *I-V* characteristic of Al-deposited ZnO step.

NH_4Cl (= 3.58×10^{-7} mole/L) at same concentration (20%) of solution. The variation of etch rates with concentration of solution is shown in Figure 9(c). It is observed that as the concentration varies from 15% to 25%, the ZnO etch rate varies from 0.16 to 0.28 µm/min. Finally, 20%NH_4OH solution with electrolytically-added Cu ions was selected for etching ZnO layer during fabrication of acoustic sensor. After etching ZnO layer using this solution, the remaining process steps were completed according to process flowchart (Figure 3).

III. Results and Discussion

The electrical reliability of step coverage in acoustic sensor fabricated by etching ZnO layer in different etchants was tested as follows:

A. ZnO etched by HCl

A SEM image of device structure fabricated using this technique is shown in Figure 10(a). Figure shows that the etching takes place in such a way that ZnO edge moves inwards toward bottom surface (instead of outward in positive slope). Because of negative slope, during deposition of Al (for top electrodes), the ZnO step is not fully covered with Al. The overall result is that the Al film is formed as a hanging structure which does not touch the bottom surface of ZnO film. The discontinuity in Al layer on ZnO step can be easily seen from this Figure. The mechanism for the negative slope formation is that the lateral etch rate is higher than vertical etch rate in case of strong acidic solutions even at lower concentration. As the etchant concentration increases, hydroniun ion concentration increases. This increase in hydronium ions is responsible for negative slope of ZnO layer. To perform the electrical testing of the fabricated device, two probes were placed, first one on the Al film below which the ZnO layer was etched in the solution and the second on the Al deposited ZnO film. Electric current from a power supply was passed through the Al film from probe 1 to probe 2. The current was slowly increased in steps to determine the maximum current that the Al film could sustain. *I-V* characteristic across Al-deposited over ZnO edge, etched by strong acid (HCl) is plotted in Figure 10(b).

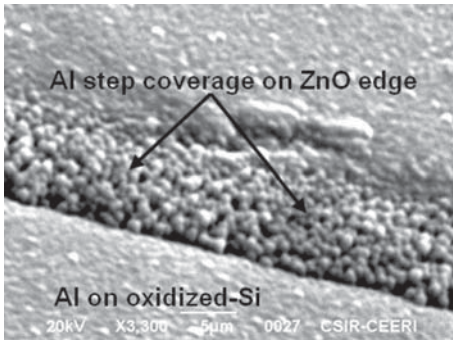

Figure 13: Al step coverage on ZnO edge produced by NH_4OH with electrolytically-added Cu ions.

It was observed that the maximum current drawn across Al deposited ZnO edge is 40 mA without any damage to the structure. When we pass the current above the maximum limit, the structure is damaged and the circuit becomes open, i.e., the current passing through the step becomes zero. Therefore, the electrical testing of the structure indicates the poor step coverage of ZnO edge in case of strong acid HCl.

B. ZnO etched by NH_4Cl with electrolytically-added Cu ions

A SEM photograph of device structure fabricated using this technique is shown in Figure 11. To perform the electrical testing of fabricated device using NH_4Cl with Cu added solution for ZnO etching, two probes were placed, first one on the Al film below which the ZnO layer was etched in the solution and the second on the Al-deposited ZnO film [Figure 12(a)]. Electric current from a power supply was passed through the Al film from probe 1 to probe 2. The current was slowly increased in steps to determine the maximum current that the Al film could sustain. It was observed that the maximum current drawn across Al deposited ZnO edge is 2.5 A without any damage to the structure. When we pass the current above the maximum limit, the structure is damaged and the circuit becomes open, i.e., the current passing through the step becomes zero. The enlarged view of Al breakage over ZnO step is shown in Figure 12(b). The *I-V* characteristic

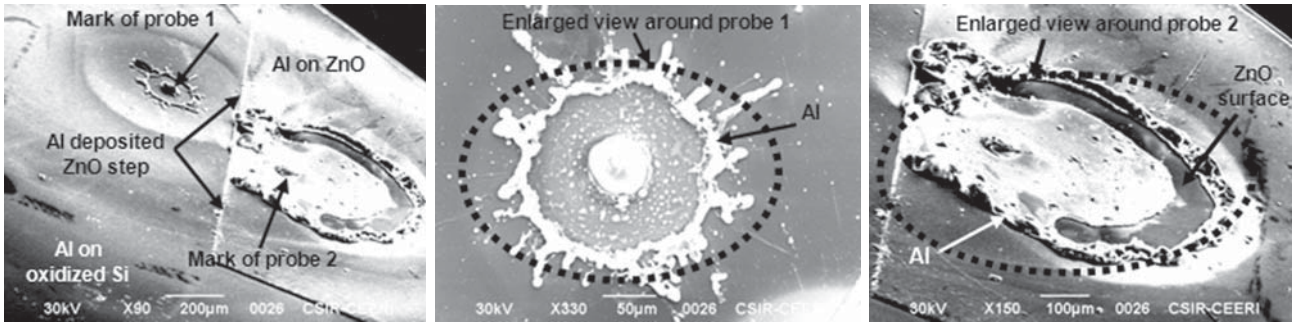

(a) (b) (c)

Figure 14: Electrical testing of structure fabricated by etching ZnO in 20%NH_4OH solution with electrolytically-added Cu ions: (a) SEM photograph of structure after passing high current, (b) enlarged view of Al breakage around probe 1, and (c) enlarged view of Al breakage around probe 2.

across Al-deposited over ZnO edge, is plotted in Figure 12(c). Therefore, the electrical testing of the structure indicates the good step coverage of ZnO edge in case of weak acid NH_4Cl with electrolytically-added Cu ions.

C. ZnO etched by NH_4OH with electrolytically-added Cu ions

A SEM photograph of device structure fabricated using this technique is shown in Figure 13. A better positive slope of ZnO edge and Al step coverage was observed in this case. To performed the electrical testing, two probes were placed, first one on the Al film below which the ZnO layer was etched in the solution and the second on the Al-deposited ZnO film [Figure 14(a)].

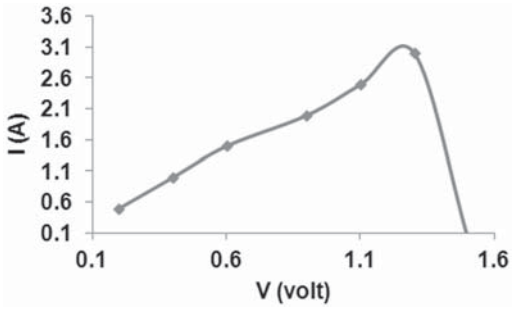

Figure 15: *I-V* characteristic of Al-deposited ZnO step in case of 20%NH_4OH with electrolytically-added Cu ions.

It was observed that the maximum current drawn across Al-deposited ZnO edge is approximately 3.0 A without any damage to the structure. When we pass the current above 3.0 A, the structure is damaged [Figure 14] and the circuit becomes open, i.e., the current passing through the step becomes zero. The SEM images clearly show that the step area remains intact although Al has spread out around the probe points at 3.0 A current. The breakage of Al around probe 1 and around probe 2 can be easily seen from Figure 14(b) and 14(c) respectively. The lifting of Al from ZnO surface (around probe 2) can be seen from Figure 14(c). The *I-V* characteristic across Al-deposited over ZnO edge, is plotted in Figure 15. The electrical testing of the structure indicates the much better step coverage of ZnO edge in case of Cu added NH_4OH as compared to Cu added NH_4Cl and strong acid HCl. A good etch rate as well as highly desirable positive slope, both were observed in case of 20% NH_4OH solution with electrolytically-added copper ions at room temperature. The ZnO etching features of NH_4OH with electrolytically-added Cu ions, NH_4Cl with electrolytically-added Cu ions and HCl are compared in Table I.

D. Response of the device

The fabricated MEMS acoustic sensors on 4-inch silicon wafer are shown in Figure 16(a). The fabricated wafer was diced using double spindle dicing machining. The microtunnel is opened to the atmosphere during dicing. A SEM image of microtunnel opening to the atmosphere is shown in Figure 16(b). The packaged device [Figure 16(c)] performed satisfactorily within SPL range 120-160 dB over a wide bandwidth 30-8000 Hz with varying acoustic pressure [Figure 17]. The maximum sensitivity of the sensor was found to be 380 µV/Pa.

IV. Conclusions

The significant features of the proposed technique for microtunnel fabrication have been discussed. On comparison, it is observed that the process in proposed technique is simplified and indeed more reliable. Overall, the proposed technique can save approximately 40 hrs processing time. It gives better yield (∼60%) in comparison to old technique (< 40%) because of absence of overlapping area between tunnel and cavity in the mask layout, and also through selective protection of masking layer by photolithography. In addition, many process steps including LPCVD silicon nitride, are avoided leading to cost-effectiveness. Avoiding shortcomings of the earlier method, the proposed method can safely be used for microtunnel formation in acoustic sensor as well as other similar MEMS structures.

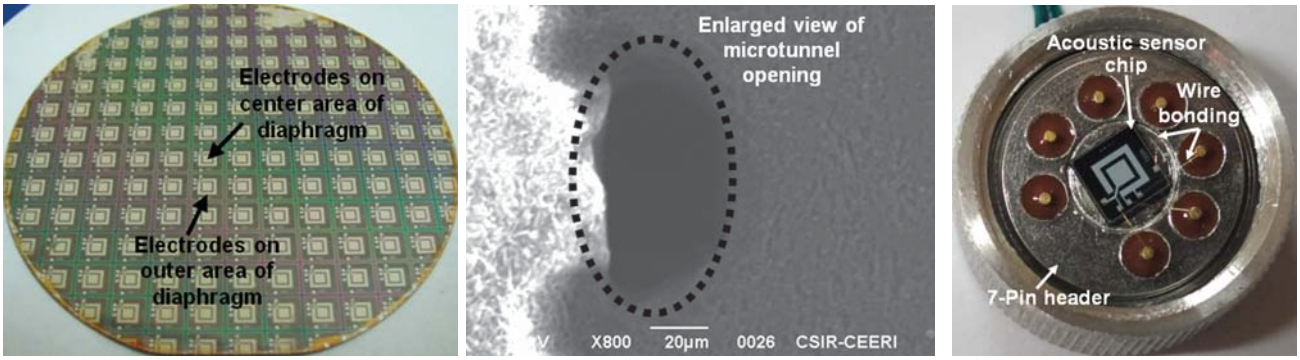

(a) (b) (c)

Figure 16: Fabricated MEMS acoustic sensor: (a) on 4-inch silicon wafer, (b) SEM images of microtunnel opening to the atmosphere, and (c) packaged device for testing.

Table I: Comparison of ZnO etching using NH_4OH with electrolytically-added Cu ions, NH_4Cl with electrolytically-added Cu ions and HCl solutions

Sl. No.	Features	NH_4OH with copper addition	NH_4Cl with copper addition	HCl
1.	ZnO etch rate	∼0.17 µm/min in 20% solution concentration at normal temperature	∼0.18 µm/min in 20 % solution concentration at normal temperature	∼3.6 µm/min in 0.25% solution concentration
2.	Etch front slope	Positive	Vertical	Negative
3.	H^+/OH^- ions concentration	3.98×10^{-13} mole/L (20% solution concentration)	3.58×10^{-7} mole/L (20% solution concentration)	0.04 mole/L (0.25% solution concentration)
4.	Maximum electric current pass through Al covered ZnO step	∼3.0 A (ZnO etched in 20% solution concentration)	∼2.5 (ZnO etched in 20% solution concentration)	∼40 mA (ZnO etched in 0.25% solution concentration)

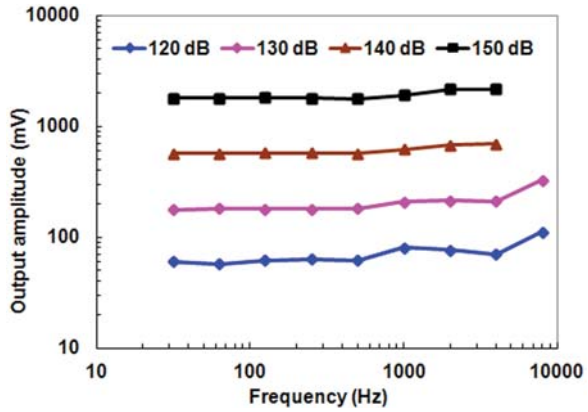

Figure 17: Output response of the device as a function of SPL.

The MEMS acoustic sensors were fabricated by etching ZnO film in three different etchants: HCl, NH_4Cl with electrolytically-added Cu ions. We have proposed and evaluated a novel wet etchant NH_4OH with electrolytically-added Cu ions and found that it is more suitable for etching ZnO film. The maximum current drawn across Al-deposited ZnO edge, etched by HCl was 40 mA, that across Cu added NH_4Cl was 2.5 A, and for Cu added NH_4OH was 3.0 A. The current-carrying capability in case of HCl is lowest (∼40 mA) because current flows only through some regions on the step, i.e., the step is partially conducting. The film is likely to breakdown during device operation, causing electrical failure. The current-carrying capability is improved with NH_4Cl, and still further in case of NH_4OH with electrolytically-added Cu ions. The same is also verified from SEM photographs of fabricated device. A good etch rate as well as highly desirable positive slope, both were obtained in case of 20% NH_4OH with electrolytically-added Cu ions. The packaged device performed well in wide frequency range 30 Hz to 8 kHz and a high sensitivity of 380 µV/Pa was achieved.

ACKNOWLEDGMENTS

The authors thank Dr. Chandra Shekhar, the Director, CSIR-CEERI, Pilani, for encouragement and guidance. They gratefully acknowledge the help received from Prof. Vinay Gupta of Delhi University, Delhi for facilitating the zinc oxide deposition.

REFERENCES

[1] P. Scheeper, J. O. GullØv, L. M. Kofoed, "A piezoelectric triaxial accelerometers", *J. Micromech. Microeng.*, vol. 6, pp. 131-133,1996.
[2] S. C. Ko, Y. C. Kim, S. S. Lee, S. H. Choi. S. R. Kim, "Micromachined piezoelectric membrane acoustic device", *Sensors and Actuators A*, vol. 103, pp. 130-134, 2003.
[3] D. L. DeVoe, A. P. Pisano, "Surface micromachined piezoelectric accelerometers (PiXLs)", *J. Microelectromechanical Syst.*, vol. 10, pp. 180-186, 2001.
[4] G. Percin, B. T. K. Yakub, "Piezoelectrically actuated flextensional micromachined ultrasound transducers", *Ultrasonics*, vol. 40, pp. 441-448, 2002.
[5] T. Xu, G. Wu, G. Zhang, Y. Hao, "The compatibility of ZnO piezoelectric film with micromachining process", *Sensors and Actuators A*, vol. 104, pp. 61-67, 2003.
[6] L. Mai, J. Y. Lee, V. S. Pham, and G. Yoon, "Design and fabrication of ZnO-based FBAR microwave devices for mobile WiMAX applications," *IEEE Microw. Wireless Compon.* Lett., vol. 17, no. 12, pp. 867–869, Dec. 2007.

[7] F. S. Hickernell, "The microstructural characteristic of thin-film zinc oxide SAW transducers," in Proc. *IEEE Ultrosonic Symp*., Nov. 1984, pp. 239–242.

[8] P. R. Ried, E. S. Kim, M. H. David, and S. R. Muller, "Piezoelectric microphone with on-chip CMOS circuits," *J. Microelectromech. Syst.*, vol. 2, no. 3, pp. 111–120, Sep. 1993.

[9] W. S. Lee, Y. C. Kim, J. S. Lee, S. W. Lee, and S. S. Lee, "Fabrication of circular diaphragm for piezoelectric acoustic devices," *J. Semicond. Technol. Sci*., vol. 5, no. 1, pp. 52–57, 2005.

[10] B. S. Li, Y. C. Liu, Z. S. Chu, D. Z. Shen, Y. M. Lu, J. Y. Zhang, and X. W. Fan, "High quality ZnO thin films grown by plasma enhanced chemical vapor deposition", *J. Appl. Phys.* vol. 91, pp. 501-504, 2001.

[11] M. D. Barankin, E. Gonzalez II, A. M. Ladwig, and R. F. Hicks, "Plasma enhanced chemical vapor deposition of zinc oxide at atmospheric pressure and low temperature," *Solar Energy Mater. Solar Cells*, vol. 91, pp. 924–930, 2007.

[12] J. B. Lee, H. J. Kim, S. G. Kim, C. S. Hwang, S. H. Hong, Y. H. Shin, N. H. Lee, "Deposition of ZnO thin films by magnetron sputtering for a film bulk acoustic resonator", *Thin Solid Films*, vol. 435, pp. 179-185, 2003.

[13] D. J. Kang, J. S. Kim, S.W. Jeong, Y. Roh, S. H. Jeong, J. H. Boo, "Structural and electrical characteristics of R.F. magnetron sputtered ZnO films", *Thin Solid Films*, vol. 475, pp. 160-165, 2005.

[14] F. Vigue, P. Vennegues, S. Vezian, M. Laugt, and J. P. Faurie, "Defect characterization in ZnO layers grown by plasma-enhanced molecular-beam epitaxy on (0001) sapphire substrates", *Appl. Phys. Lett.*, vol. 79, pp. 194-196, 2001.

[15] S. L. King, J. G. E. Gardeniers, Ian W. Boyd, "Pulsed-laser deposited ZnO for device applications", *Applied Surface Science*, 96-98, pp. 811-812, 1996.

[16] T. Ohshima, R. K. Thareja, T. Ikegami, K. Ebihara, "Preparation of ZnO thin films on various substrates by pulsed laser deposition", *Surface and Coatings Technology*, 169 –170, pp. 517–520, 2003.

[17] S. H. Nam, S. H. Jeong, and J. H. Boo, "Growth Behavior and Characteristics of One Dimensional ZnO Nanostructures by Metalorganic Chemical Vapor Deposition", *Journal of Nanoscience and Nanotechnology*, vol. 11, pp. 1648–1651, 2011.

[18] M. Tomar, V. Gupta, K. Sreenivas, and A. Mansingh, "Temperature Stability of ZnO Thin Film SAW Device on Fused Quartz", *IEEE transactions on device and materials reliability*, vol. 5, no. 3, sept. 2005.

[19] X. Y. Du1, Y. Q. Fu1, S. C. Tan, J. K. Luo, A. J. Flewitt, S. Maeng, S. H. Kim, Y. J. Choi, D. S. Lee, N. M. Park, J. Park, W. I. Milne, "ZnO film for application in surface acoustic wave device", *IOP Publishing, Journal of Physics:* Conference Series 76 (2007) 012035.

[20] J. M. Lee, K. M. Chang, K. K. Kim, W. K. Choi, and S. J. Park, "Dry Etching of ZnO Using an Inductively Coupled Plasma", *Journal of Electrochem. Soc.*, vol. 148, pp. G1-G3, 2001.

[21] J. W. Bae, C. H. Jeong, H .K. Kim, K. K. Kim, N. G. Cho, T. Y. Seong, S. J. Park, I. Adesida and G. Y. Yeom, "High-Rate Dry Etching of ZnO in $BCl_3/CH_4/H_2$ Plasmas", *Jpn. J. Appl. Phys*. vol. 42, pp. L 535–L 537, Part 2, No. 5B, May 2003.

[22] H. K. Kim, J. W. Bae, K. K. Kimb, S. J. Parkb, T. Y. Seong, I. Adesida, "Inductively-coupled-plasma reactive ion etching of ZnO using BCl_3-based plasmas and effect of the plasma treatment on TiyAu ohmic contacts to ZnO", *Thin Solid Films*, vol. 447 –448, pp.90-94, 2004.

[23] M. Mehta, M. Ruth, and K. A. Piegdon, "Inductively coupled plasma reactive ion etching of bulk ZnO single crystal and molecular beam epitaxy grown ZnO films", *J. Vac. Sci. Technol. B*, vol. 27, no.5, pp. 2097-2101, Sep/Oct 2009.

[24] M. S. Wu, A. Azuma, T. Shiosaki, and A. Kawabata, "Low-loss ZnO optical waveguides for SAW-AO applications," *IEEE Trans. Ultrason., Ferroelectr. Freq. Control*, vol. 36, pp. 442–445, July 1989.

[25] J. G. E. Gardeniers, Z. M. Rittersma, and G. J. Burger, "Preferred orientation and piezoelectricity in sputtered ZnO films," *J. Appl. Phys*., vol. 83, pp. 7844–7854, June 1998.

[26] M. Prasad, R. P. Yadav, V. Sahula, V.K. Khanna, and C. Shekhar "Controlled Chemical Etching of ZnO Film for Step Coverage in MEMS Acoustic Sensor," *J. Microelectromech. Syst., Lett.*, vol. 21, no. 3, pp. 517–519, Jun e 2011.

[27] M. Prasad, V. Sahula and V.K. Khanna, "Design and fabrication of Si-diaphragm, ZnO piezoelectric film-based MEMS acoustic sensor using SOI wafers", *IEEE Transactions on Semiconductor Manufacturing*, vol. 26, no. 2, pp. 233-241, May 2013.

[28] J. W. Kwon and E. S. Kim, "Fine ZnO patterning with controlled sidewall etch front slope," *J. Microelectromech. Syst.*, vol. 14, no. 3, pp. 603–609, June 2005.

[29] H. Maki, T. Ikoma, I. Sakaguchi, N.Ohashi, H. Haneda, J. Tanaka, N. Ichinose, "Control of surface morphology of ZnO (0 0 0 1¯) by hydrochloric acid etching", *Thin Solid Films*, vol. 411, pp. 91-95, 2002.

[30] S. C. Chang, D. B. Hicks, and R. C. Laugal, "Pattering of zinc oxide thin films," in Proc. *IEEE Solid-State Sensor and Actuator Workshop*, Hilton Head Island, SC, Jun. 21–25, pp. 41–45, 1992.

[31] J. Sun, J. Bian, H. Liang, J. Zhao, L. Hu, Z. Zhao, W. Liu, G. Du, "Realization of controllable etching for ZnO film by NH_4Cl aqueous solution and its influence on optical and electrical properties", *Applied Surface Science*, vol. 253, pp. 5161–5165, 2007.

[32] J. D. Bradley and C. W. Bruce, "Novel MEA Platform with PDMS Microtunnels Enables Detection of Action Potential Propagation from Isolated Axons in Culture", *Lab Chip*., 9(3), Feb 2009.

[33] D. Kim, D. W. Lee, W. Choi, J. B. Lee, "A Super-Lyophobic PDMS Micro-tunnel as a Novel Microfluidic Platform for Oxidized Galinstan", *IEEE MEMS 2012 Conference*, Paris, France, 29 January - 2 February 2012.

[34] D. Bhusari, H. A. Reed, M. Wedlake, A. M. Padovani, S. A. B. Allen, and P. A. Kohl, "Fabrication of Air-Channel Structures for Microfluidic, Microelectromechanical, and Microelectronic Applications", *Journal of Microelectromechanical Systems*, vol. 10, no. 3, pp. 400-408, 2001.

[35] J. L. H. Chau and K. L. Yeung, "Zeolite microtunnels and microchannels", *Chem. Commun.* vol. 9, pp. 960–961, 2002.

[36] H. J. G. E. Gardeniers, R. Luttge, E. J. W. Berenschot, M. J. de Boer, S. Y. Yeshurun, M. Hefetz, R. V. Oever, and A. V. D. Berg , "Silicon Micromachined Hollow Microneedles for Transdermal Liquid Transport", *Journal of Microelectromechanical Systems*, vol. 12, no. 6, pp. 855-862, 2012.

[37] C. Fu, C. Hung, H. Huang, "A novel and simple fabrication method of embedded SU-8 micro channels by direct UV lithography", *Institute of Physics Publishing, Journal of Physics:* Conference Series 34, pp. 330–335, 2006.

[38] A. Arora, A. Arora, V. K. Dwivedi, P.J. George, K. Sreenivas, V. Gupta, "Zinc oxide thin film-based MEMS acoustic sensor with tunnel for pressure compensation", *Sensors and Actuators A*, vol. 141, pp. 256–261, 2008.